*Article*

# Stray Light Analysis and Suppression of Taiji Telescope for Space Gravitational Wave Detection Based on Phase Noise Requirement

**Benliang Sang** [1,2]**, Xiaoqin Deng** [1,2]**, Wei Tao** [1,2]**, Yuqing Diao** [1,2] **and Wei Sha** [1,2,*]

[1] Changchun Institute of Optics, Fine Mechanics and Physics, Chinese Academy of Sciences, Changchun 130033, China
[2] University of Chinese Academy of Sciences, Beijing 100049, China
[*] Correspondence: shawei@ciomp.ac.cn

**Abstract:** The telescope is the core device for space gravitational wave detection. It is responsible for receiving signal light and emitting outgoing light simultaneously. When the high-energy outgoing laser passes through the telescope, it would produce stray light, which would interfere with the phase measurement and generate phase noise. Therefore, it is necessary to analyze and suppress the stray light of the telescope. In this paper, the requirement of point source transmittance (PST) of the Taiji telescope is obtained through theoretical derivation, which is less than $4 \times 10^{-10}$. Through a complete analysis of stray light, we determined that the M4 was the largest source of stray light under the condition that the roughness of each optical surface is equal, which accounted for 67.22%. We also determined the most lenient requirements for surface roughness $\sigma_\lambda$, and found that when $\sigma_\lambda$ of the M1, M2, M3, and M4 were 20 Å, 4 Å, 1 Å, and 1 Å, respectively, the PST was $3.89 \times 10^{-10}$, which met the PST requirement. Next, we calculated the effect of particulate contamination on the PST, and based on the results of our analysis, we determined that the cleanliness level of the testing and storage environment of the Taiji telescope was better than 300. Finally, we evaluated the changes in the PST caused by the damage of micrometeoroids, and the analysis results showed that the stray light level would not change significantly during the service period of the Taiji Telescope.

**Keywords:** stray light analysis; Taiji telescope; space gravitational wave; space gravitational wave detection; surface roughness; particulate contamination; micrometeoroid

## 1. Introduction

In 2016, LIGO announced its detection of gravitational wave events [1], which is the first time that humans achieved direct detection of gravitational waves, thus, Einstein's prediction about gravitational waves was confirmed. The ground-based gravitational wave detectors represented by LIGO are affected by ground vibrations, gravitational gradient noise, and short interferometric arm lengths, resulting in their low detection sensitivity, which can only detect gravitational waves at frequencies above 10 Hz [2]. However, for most of the gravitational wave sources in the universe, the frequency range of gravitational waves is between 0.1 mHz and 1 Hz [3,4]. To achieve the detection of low-frequency gravitational wave signals, they must be free from the limitations of the ground environment to develop space gravitational wave detection. With high detection sensitivity, space gravitational wave detection can achieve the detection of more gravitational wave sources, including early cosmic phase transitions, cosmic strings, and dense binary systems. The detection of these sources can provide key information for the research of the early universe, unified field theory, and the evolution of the universe [5].

The Taiji Project is a space gravitational wave detection project proposed by the Chinese Academy of Sciences, aiming to detect picometer-level space gravitational wave

signals within the frequency range of 0.1 mHz to 1 Hz [6–8]. Taiji plans to launch three satellites to form three laser interference links, each with a length of 3 million kilometers [9,10]. In order to establish an effective laser transmission path between the two satellites, laser transceiver telescopes are designed at both ends of each interferometric link.

The laser transceiver has two functions: one is to expand the outgoing beam from the scientific interferometer with a diameter of 2 mm into a collimated beam with a diameter of 200 mm, which is transmitted to the remote detector; the other is to narrow the signal beam and transmit it to the interferometer optical platform [11]. When the telescope emits the local laser, the laser power at the entrance pupil is close to 2 W, while the power of the signal beam received by the telescope from the remote detector is about 300 pW [9]. Backscattering is inevitable when a high-power outgoing beam passes through the telescope, and the backscattered light would interfere with the local reference beam, thus any phase fluctuation of the backscattered light would affect the measurement of the interference signal [12,13]. Therefore, it is necessary to analyze and suppress the backscattered light of the telescope.

In order to reduce the level of backscattered light, the optical system of the Taiji Telescope adopts an unobstructed off-axis four-mirror optical system. Due to the added tilt of the secondary mirror, the narcissus reflection is completely avoided [14,15]. However, non-zero surface roughness is unavoidable during the manufacturing process of optical surfaces, and there should also be the possibility of contamination of optical surfaces, both of which would affect backscattering [16,17]. In addition, the telescope will face the risk of micrometeoroid impacts once in orbit [18–20]. The high-speed impact of micrometeoroids will cause damages to optical surfaces, leading to increased levels of stray light.

In this paper, the numerical analysis of the backscattering of the Taiji telescope has been carried out, and the influence mechanism of the backscattered light on the phase has been clarified through theoretical derivation with the requirements for the stray light of the telescope obtained. Subsequently, the precise scattering path of the stray light has been determined by the analysis of stray light on the Taiji telescope. The effect of optical surface roughness and cleanliness on the level of stray light has been studied. In addition, we have also made predictions about the possible effects of micrometeoroids on the telescope, and the corresponding changes in stray light levels have been obtained. Finally, the optimal combination of optical surface roughness has been recommended for the construction of the telescope, and specific requirements for the cleanliness level of the environment have also been put forward.

## 2. Theoretical Analysis of Phase Noise Generated by the Backscattered Light

The off-axis four-mirror optical system used in the Taiji Telescope is shown in Figure 1a, where the primary mirror is a paraboloid, the secondary mirror is a hyperboloid, and the third and fourth mirrors are both spherical [21]. The detailed parameters are shown in Table 1. The Taiji interferometer adopts a balanced orthogonal four-quadrature detection scheme to detect phase signals, and its transmitting and receiving optical paths are shown in Figure 1b. For the transmitting optical path, the beam emitted by the frequency-stabilized laser is divided into two beams by the polarization beam splitter, one of which is used as the local reference beam (polarization state is s), and the other forms the outgoing beam (polarization state is p). For the receiving optical path, the signal light becomes s light after passing through a 1/4 wave plate twice, and then interferes with the local reference beam after multiple reflections. It should be noted that both the frequency and polarization states of the backscattered light generated by the outgoing beam are consistent with the local reference beam, which means that it can interfere with the local reference beam, resulting in an additional phase. If the additional phase was a constant, it would have very little effect on the phase measurement, but in reality, the scattered light is affected by variations in the telescope's optical length. Therefore, the additional phase caused by the scattered light is also variable, that is, the phase noise.
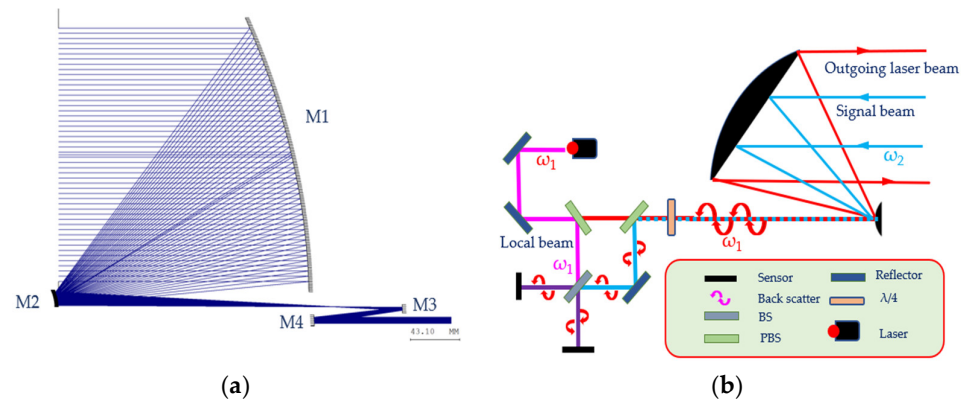
**Figure 1.** (**a**) Schematic diagram of the off-axis four-mirror optical system adopted by the Taiji Telescope. Compared with the coaxial optical system, its ability to suppress stray light is stronger. (**b**) Schematic diagram of the light field distribution in the telescope. The figure shows the outgoing laser light (red), signal light (blue), and backscattered light (wave) of the Taiji telescope.

**Table 1.** Parameters of the optical system of Taiji telescope.

|  | Parameter | Requirement |
|---|---|---|
| 1 | Optical aperture | 200 mm |
| 2 | Optical efficiency | 0.853 |
| 3 | Working wavelength | 1064 nm |
| 4 | Field-of-View (spatial acquisition) | $\pm$200 µrad |
| 5 | Field-of-View (science) | $\pm$20 µrad out-of-plane |
|  |  | $\pm$8 µrad in-plane |
| 6 | Surface Flatness | $\lambda/70$ RMS |
| 7 | Wavefront quality over science field of view | $\lambda/30$ RMS |

As shown in Figure 2, we use $E_l$, $E_b$, and $E_s$ to denote the electric field complex amplitude of the local beam, the backscattered beam, and the signal beam, respectively. All three beams of light can interfere with each other. Furthermore, the distributions of the light fields $E_1$ and $E_2$ are described by Equations (1) and (2).

$$E_1 = E_L e^{(i\omega_1 t)} + E_S e^{i(\omega_2 t + \varphi_S + \frac{\pi}{2})} + E_B e^{i(\omega_1 t + \varphi_B + \frac{\pi}{2})} \tag{1}$$

$$E_2 = E_L e^{(i\omega_1 t + \frac{\pi}{2})} + E_S e^{i(\omega_2 t + \varphi_S)} + E_B e^{i(\omega_1 t + \varphi_B)} \tag{2}$$
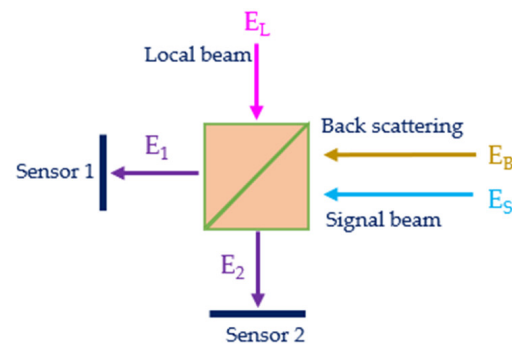


**Figure 2.** Schematic diagram of balanced orthogonal detection.

According to the design of the Taiji interferometer, the output optical power $P_O$ of the frequency-stabilized laser is 2 $W$, the optical power of the local beam $P_L = 2 \times 10^{-3}$ $W$, and the optical power of the signal light $P_S = a^2 P_L = 3 \times 10^{-10}$ $W$. For the convenience of calculation, we introduce the parameter $a^2$, where $a^2$ is a constant with a value of $1.5 \times 10^{-7}$. Similarly, the optical power of stray light $P_B = u^2 P_L$, where $u^2 \ll 1$. Since the optical power $P$ is proportional to the square of the electric field, $P \propto E^2$, we rewrite Equations (1) and (2) into the following form:

$$E_1 = \sqrt{P_L} e^{i\omega_1 t} \left( 1 + a_1 e^{i(\Delta \omega t + \varphi_S + \frac{\pi}{2})} + u_1 e^{i(\varphi_B + \frac{\pi}{2})} \right) \tag{3}$$

$$E_2 = \sqrt{P_L} e^{i\omega_1 t} \left( e^{i\frac{\pi}{2}} + a_2 e^{i(\Delta \omega t + \varphi_S)} + u_2 e^{i\varphi_B} \right) \tag{4}$$

where $\Delta \omega = \omega_2 - \omega_1$, $u_1^2 + u_2^2 = u^2$, $a_1^2 + a_2^2 = a^2$. Since the common divisor $\sqrt{P_L} e^{i\omega_1 t}$ has no effect on the calculation of phase, we omit it when calculating the current signal below.

The output currents $I_1$, $I_2$ of the two detectors are proportional to $E_1{}^2$, $E_2{}^2$, respectively. Here we assume that the conversion efficiency of the detector is 1, and only the AC signal is output. The AC terms of $I_1$, $I_2$ are described by Equations (5) and (6), where $a_1 \approx a_2$.

$$I_1(t) = -2u_1 \sin(\varphi_B) - 2a_1 \sin(\Delta \omega t + \varphi_S) + 2a_1 u_1 \cos(\Delta \omega t + \varphi_S - \varphi_B) \tag{5}$$

$$I_2(t) = -2u_2 \sin(\varphi_B) - 2a_2 \sin(\Delta \omega t + \varphi_S) + 2a_2 u_2 \cos(\Delta \omega t + \varphi_S - \varphi_B) \tag{6}$$

The final output signal can be obtained by $I_1 - I_2$, and the measurement equation for the phase $\varnothing$ of the interference signal is described by Equation (7) [22], where $\widetilde{u} = (a_1 u_1 - a_2 u_2)/(a_1 + a_2) \approx (u_1 - u_2)/2$. Let $\varphi_n = \widetilde{u} \sin(\varphi_B) + \widetilde{u}^2 \sin(\varphi_B) \cos(\varphi_B)$, then $\varphi_n$ is the phase noise.

$$\varnothing = \varphi_S + \frac{\pi}{2} + \widetilde{u} \sin(\varphi_B) + \widetilde{u}^2 \sin(\varphi_B) \cos(\varphi_B) \tag{7}$$

Here, we introduce a constant $\delta$ to represent the splitting ratio error of BS (as shown in Figure 2), then $u_1 = \sqrt{\frac{1+\delta}{2}} u$, $u_2 = \sqrt{\frac{1-\delta}{2}} u$. After Taylor expansion for $u_1$ and $u_2$, respectively, and keeping only the low-order terms, we get $u_1 \approx \frac{2+\delta}{2\sqrt{2}} u$, $u_2 \approx \frac{2-\delta}{2\sqrt{2}} u$. For the phase noise $\varphi_n$, its second-order term is tiny and can be ignored. Thus, the simplified phase noise is described by Equation (8).

$$\varphi_n = \frac{\delta u \sin(\varphi_B)}{2\sqrt{2}} \tag{8}$$

Here, we use variance $\sigma^2$ to describe the variation of the phase noise $\varphi_n$. For convenience, the backscattered light can be regarded as the sum of $n$ individual rays [22], and it is assumed that the distribution of all these rays obey $\frac{1}{\pi\sqrt{1-x_j^2}}$, then:

$$u \sin(\varphi_B) = \sum_{j=1}^{n} u_j \sin\left(\varphi_B^j\right) \tag{9}$$

In order to calculate the variance, we first need to calculate the mean of the above formula. The mean calculation process is as follows:

$$\langle u \sin(\varphi_B) \rangle = \left\langle \sum_{j=1}^{n} u_j \sin\left(\varphi_B^j\right) \right\rangle = \sum_{j=1}^{n} u_j \left\langle \sin\left(\varphi_B^j\right) \right\rangle = \sum_{j=1}^{n} u_j \int_{-1}^{1} \frac{\sin\left(\varphi_B^j\right)}{\pi\sqrt{1-x_j^2}} dx_j = 0 \tag{10}$$

According to the definition of variance and the previous definition of the optical power of stray light and local beam, $P_B = u^2 P_L$, we can get:

$$var[u \sin(\varphi_B)] = \left\langle \sum_{j=1}^{n} \left( u_j \sin\left(\varphi_B^j\right) - 0 \right)^2 \right\rangle = \sum_{j=1}^{n} u_j^2 \left\langle \sin^2\left(\varphi_B^j\right) \right\rangle = \frac{1}{2} \sum_{j=1}^{n} u_j^2 = \frac{1}{2} \frac{P_B}{P_L} \tag{11}$$

Therefore, the variance of the phase noise is described by Equation (12).

$$\sigma^2 = \frac{\delta P_B}{4\sqrt{2} P_L} \tag{12}$$

According to the requirements of Taiji Project, the phase noise caused by the backscattered light should be less than 1 pm, and the spectral error of BS should be less than 0.001. According to Equation (12), the requirement for the backscattered light energy of the telescope can be obtained.

$$\frac{P_B}{P_L} \leq 2 \times 10^{-7} \tag{13}$$

There are various evaluation functions for stray light, the most commonly used of which is point source transmittance (PST) [23–25]. For the stray light analysis to be performed in this paper, the PST that meets the phase noise requirement is:

$$\text{PST}(\theta) = \frac{P_B}{P_O} < 4 \times 10^{-10} \tag{14}$$

## 3. Calculation Method of the Backscattered Light of the Taiji Telescope

Since the scientific field of view of the Taiji telescope is extremely small ($\pm 8$ $\mu$rad), and there is no mechanical structure in the field of view of the Taiji telescope, we only consider the scattering from the optical surface when performing the stray light analysis. In addition, since the scattering is random, we use the scattered light aiming method for stray light analysis in order to improve the efficiency of simulation analysis. The stray light simulation software used in this paper is ASAP.

### 3.1. Analysis of the Proportion of Scattered Light Energy by the Mirrors of the Taiji Telescope

Before performing surface roughness and cleanliness analysis, it is necessary to clarify the contribution of each optical surface to scattering. We placed a parallel light source with a wavelength of 1064 nm in front of the telescope's exit pupil and set a fully absorbing target surface (1 mm in diameter) at the exit pupil to receive the backscattered light. At the same time, we also set the corresponding light aiming area. In this paper, the Harvey–Shack model is used to describe the scattering under different surface roughness. The Harvey–Shack model is a common model for BSDF modeling of optical surfaces and is supported by most stray light analysis software [26–28]. In the analysis of this section, we set the roughness of each optical surface to 5 Å.

The scattering energy analysis results of each mirror are shown in Table 2, and the main scattering paths are shown in Figure 3. We can see that the scattering energy from the M4 and the M3 accounts for a considerable part. Among them, the M4 produces the first-order scattering with the largest energy, while the scattering energy from the M1 is the lowest.

**Table 2.** The proportion of scattered energy of each mirror.

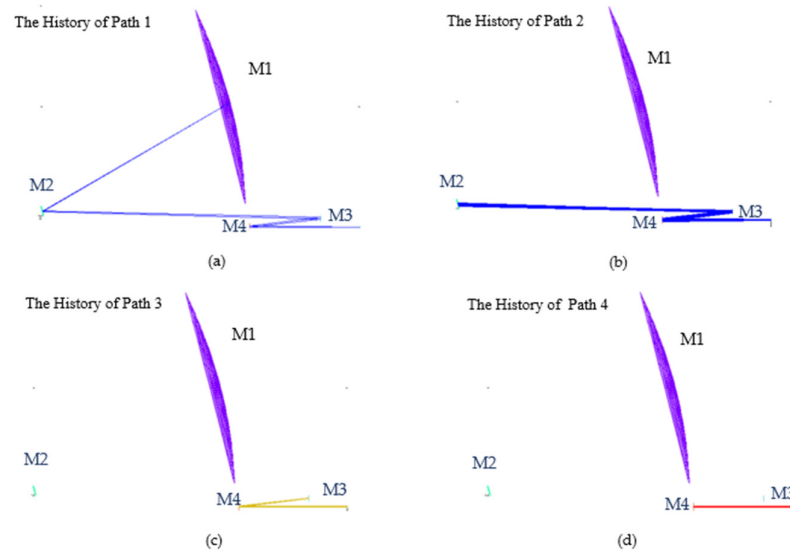| Optical Surface | Scattered Energy | Percentage |
|:---:|:---:|:---:|
| M1 | $2.27 \times 10^{-12}$ | 0.03% |
| M2 | $1.35 \times 10^{-10}$ | 1.72% |
| M3 | $2.42 \times 10^{-9}$ | 31.02% |
| M4 | $5.25 \times 10^{-9}$ | 67.22% |

**Figure 3.** Main scattering paths of the Taiji telescope. (**a**) In scattering path 1, the scattering energy comes from M1, accounting for 0.03%. (**b**) In scattering path 2, the scattered energy comes from M2, accounting for 1.72%. (**c**) In scattering path 3, the scattered energy comes from M3, accounting for 31.02%. (**d**) In scattering path 4, the scattered energy comes from M4, accounting for 67.22%.

### 3.2. Analysis of the Backscattering Caused by Surface Roughness

It is impossible for the optical surface to be perfectly smooth after processing. When light hits the reflector, the reflected light exhibits a scattering phenomenon centered on the mirror. The degree of scattering is usually characterized by the bidirectional scattering distribution function (BSDF). Since the measurement of the BSDF is complex and expensive [29,30], while the measurement of surface roughness $\sigma_\lambda$ is very convenient, the relationship between $\sigma_\lambda$ and the BSDF needs to be established before the stray light analysis. The BSDF is defined as the ratio of scattering brightness to incident illuminance. In this paper, the Harvey–Shack model is used to describe the BSDF, and its specific expression is shown in Equation (15) [31], where $b_0$, $s$ and $l$ are all constants.

$$\mathrm{BSDF}\left(\vec{\beta}, \vec{\beta_0}\right) = b_0[1 + \left(\frac{\left|\vec{\beta} - \vec{\beta_0}\right|}{l}\right)^2]s/2 \tag{15}$$

Total integrated scattering (TIS) is the ratio of scattered energy to total reflected energy. For a polished optical surface, the surface roughness $\sigma_\lambda \ll \lambda$. The relationship between TIS and $\sigma_\lambda$ can be described by Equation (16) [32].

$$\mathrm{TIS} \approx \left[\frac{4\pi\sigma_\lambda \cos(\theta_i)}{\lambda}\right]^2 \tag{16}$$

According to the definitions of TIS and BSDF, TIS is equal to the integral of BSDF over the solid angle in hemispherical space. Meanwhile, it can be seen from the calculation formula of TIS that its value is maximum when the incident angle is zero. Therefore, if the worst case is considered, combined with Equation (15) yields:

$$\mathrm{TIS} = \begin{cases} \frac{2\pi b_0}{l^s(s+2)}\left[\left(1 + l^2\right)^{\frac{s+2}{2}} - l^{s+2}\right], s \neq -2, \\ \pi b_0 l^2 ln\left(1 + \frac{1}{l^2}\right), s = -2. \end{cases} \tag{17}$$

Combining Equations (16) and (17), the relationship between $\sigma_\lambda$ and the Harvey–Shack model can be obtained.

$$\sigma_\lambda^2 = \begin{cases} \frac{b_0\lambda^2}{8\pi l^s(s+2)}\left[(1+l^2)^{\frac{s+2}{2}} - l^{s+2}\right], s \neq -2, \\ \frac{b_0 l^2 \lambda^2}{16\pi} ln\left(1 + \frac{1}{l^2}\right), s = -2. \end{cases} \quad (18)$$

The values of the parameters of the Harvey–Shack model for different surface roughness are given in Table 3. The parameter s is closely related to the optical surface polishing process and usually fluctuates in the range of $-2.5$ to $-0.5$ [33]; here, we take the typical value of $s = -1.5$. In addition, the power spectral density of the polished optical surface generally has fractal characteristics, satisfying $l \ll \left|\vec{\beta} - \vec{\beta_o}\right|$. Therefore, the value of $l$ must be small enough to ignore its influence on TIS; here, we take $l = 0.01$. Figure 4 shows the BSDF distribution when the value of $b_0, l$, and $s$ are, respectively, 0.013, 0.01, and $-1.5$, and the scattering angle is $30°$.

**Table 3.** The values of the parameters of the Harvey–Shack model corresponding to different $\sigma_\lambda$.

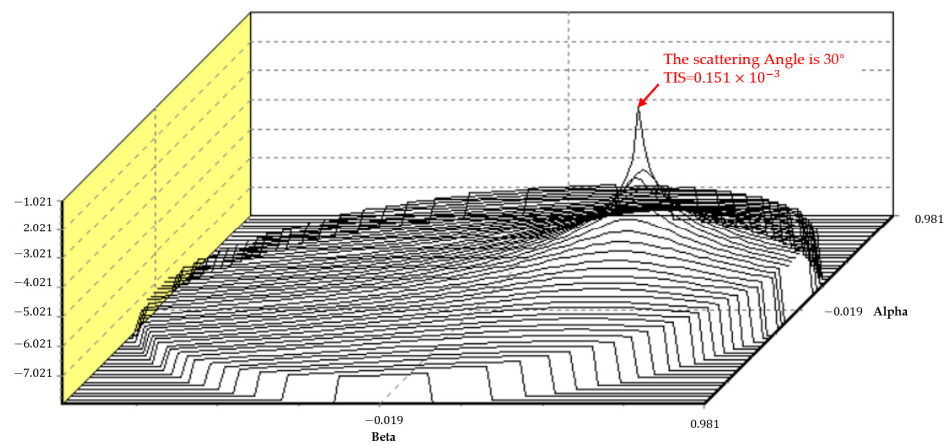| Surface Roughness (Å) | Harvey–Shack Model Parameters | | |
|---|---|---|---|
| | $b_0$ | $l$ | $s$ |
| 10 | $1.3 \times 10^{-2}$ | 0.01 | $-1.5$ |
| 5 | $3 \times 10^{-3}$ | 0.01 | $-1.5$ |
| 4 | $2 \times 10^{-3}$ | 0.01 | $-1.5$ |
| 3 | $1.1 \times 10^{-3}$ | 0.01 | $-1.5$ |
| 2 | $5 \times 10^{-4}$ | 0.01 | $-1.5$ |
| 1 | $1.3 \times 10^{-4}$ | 0.01 | $-1.5$ |



**Figure 4.** The BSDF distribution diagram when $b_0 = 0.013$, $l = 0.01$, and $s = -1.5$ and the scattering angle is 30 degrees.

According to the contribution of each mirror to PST, a different surface roughness can be assigned to each optical surface to obtain the most lenient surface roughness distribution that can meet the requirements. The corresponding stray light analysis results are shown in Table 4. As pointed out in the previous section, the contribution of the primary mirror to PST is minimal, so the surface roughness can be relaxed to 20 Å for M1, 4 Å for M2, and 1 Å for M3 and M4. Under this condition, the PST is $3.89 \times 10^{-10}$, which can meet the requirement for PST. Figure 5 shows the intensity distribution of the detector in this case.

**Table 4.** PST analysis results of optical surfaces under different surface roughness.

| M1 | M2 | M3 | M4 | PST |
|----|----|----|----|-----|
| 25 | 4 | 1 | 1 | $4.05 \times 10^{-10}$ |
| 20 | 5 | 1 | 1 | $4.23 \times 10^{-10}$ |
| 20 | 4 | 1 | 1 | $3.89 \times 10^{-10}$ |
| 10 | 4 | 1 | 1 | $3.70 \times 10^{-10}$ |
| 10 | 4 | 2 | 1 | $7.06 \times 10^{-10}$ |
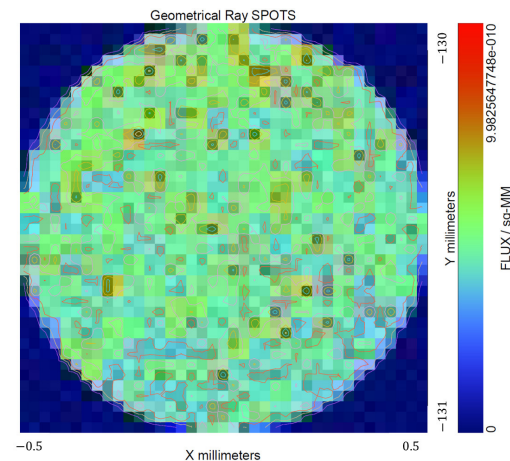


**Figure 5.** The light intensity distribution diagram of the detector at the most lenient surface roughness distribution.

### 3.3. Analysis of the Backscattering Caused by Particulate Contamination

For the optical system with a wavelength of 1064 nm, the impact of particle contamination on the BSDF of the optical surface cannot be ignored, but it is very difficult to simulate stray light on a non-ideal optical surface contaminated by particles. Since the distribution of particles and the undulation of the optical surface are random, it is quite challenging to obtain a BSDF equation that takes into account the surface roughness and particle contamination factors. Therefore, this paper only considers the situation of particle contamination on ideal optical surfaces and obtains the control level of environmental cleanliness by analyzing the stray light generated by particle contamination. In other words, at this cleanliness, we can believe that the PST of the Taiji telescope is mainly affected by the surface roughness, while the scattered energy contributed by particle contamination can be neglected.

Paul Spyak and William Wolfe elaborated in their paper that MIE scattering can be used to simulate the surface scattering of mirrors polluted by particles [34], which has been widely used. This paper focuses on the relationship between scattering and the distribution of particle size, since both the incident wavelength (1064 nm) and the incident medium (air or vacuum ($n = 1.0 + 0i$)) are determined, while the only unknown parameter in the calculation of this paper is the refractive index of the particle. According to the paper by Michael G. Dittman et al., the refractive index of the particle is not an essential factor in the MIE scattering model [35], but can be replaced by an approximation. In this paper, the refractive index of particulate contamination used is $n = 1.53 + 0.001i$.

The BSDF of an optical surface polluted by particles is closely related to the actual distribution of particles on its surface. The distribution of standard particles on the clean surface is defined in CC1246 [36]. The number ($N$) of particles with a diameter greater than d per square foot is described by Equation (19), where $CL$ represents cleanliness, generally taking $h$ as 0.926 for a clean surface and 0.383 for an uncleaned surface. By special transformation of Equation (19), the number of particles $N(d)$ with a particle size of $d$ per square foot can be obtained, and its expression is shown in Equation (20).

$$\log_{10} N = h\left(\log_{10}^2 CL - \log_{10}^2 d\right) \tag{19}$$

$$N(d) = 10^{h(\log_{10}^2 CL1 - \log_{10}^2 d)} - 10^{h[\log_{10}^2 CL1 - \log_{10}^2 (d+1)]} \tag{20}$$

In addition, the percentage space coverage $f$ is required for analysis using ASAP, which is related to cleanliness and is described by Equation (21). When $h$ is taken as 0.926, $K = -7.245$, while when $h$ is taken as 0.383, $K = -5.683$.

$$f = 10^{K + |h| log_{10}^2 (CL) - 2} \tag{21}$$

The percentage space coverage $f$ used in this simulation is shown in Table 5. Figure 6 shows the BSDF for an ideal optical surface with particle diameter from 1 to 200 μm at 500 cleanliness level.

**Table 5.** Percentage space coverage at different cleanliness levels.

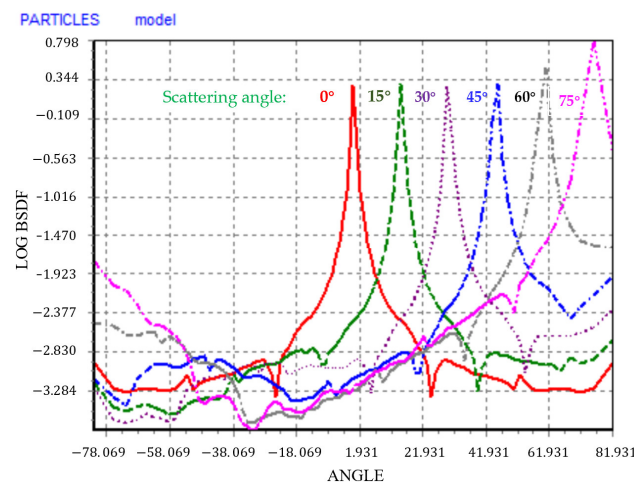| Cleanliness Level (CC1264) | Space Coverage | Cleanliness Level (CC1264) | Space Coverage |
|---|---|---|---|
| 100 | $2.88 \times 10^{-6}$ | 400 | $1.11 \times 10^{-3}$ |
| 200 | $4.55 \times 10^{-5}$ | 600 | $8 \times 10^{-3}$ |
| 300 | $2.74 \times 10^{-4}$ | 1000 | $1.13 \times 10^{-1}$ |



**Figure 6.** BSDF calculation results of an ideal optical surface at a cleanliness level of 500.

It has become a standard operation to clean the optical surface with high-speed flowing carbon dioxide gas [37]. In this way, it is effortless to clean particles with a diameter greater than 200 μm [38], so we assume that the particle diameter is between 1 um and 200 μm. Each measurement of the PST is done with a different cleanliness level that is applied to all the mirrors in the Taiji telescope, and the results of the calculation are shown in Table 6. When the cleanliness level is 300, the PST is $3.55 \times 10^{-12}$, which was two orders of magnitude below the required value. At this time, we can determine that the environmental control level of the Taiji telescope needs to be better than 300. Figure 7 shows the light intensity distribution of the detector at a cleanliness level of 300.

**Table 6.** PST analysis results of optical surfaces at different cleanliness levels.

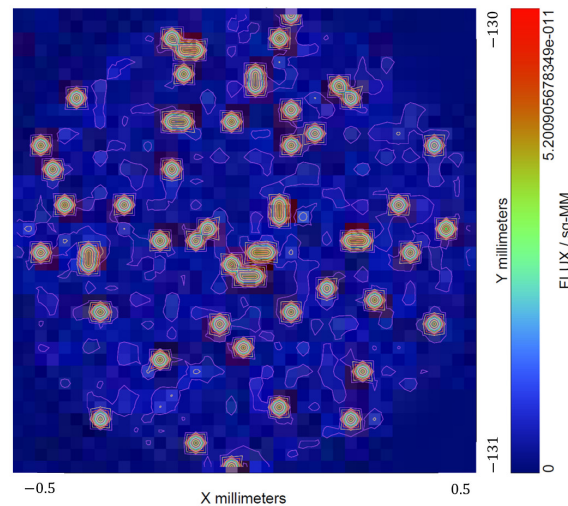| Cleanliness Level (CC1264) | PST |
|:---:|:---:|
| 100 | $3.73 \times 10^{-14}$ |
| 200 | $5.89 \times 10^{-13}$ |
| 300 | $3.55 \times 10^{-12}$ |
| 500 | $4.15 \times 10^{-11}$ |
| 1000 | $1.46 \times 10^{-9}$ |



**Figure 7.** Light intensity distribution diagram of the detector when the cleanliness level is 300.

## 4. Evaluation of the Variation of Backscattered Light of the Taiji Telescope in Orbit

The space environment where the Taiji Telescope is located is not completely clean; there are many high-speed flying particles called micrometeoroids. The high-speed impact of micrometeoroids will cause damage to the unobstructed mirror. Since the primary mirror M1 of the Taiji Telescope is directly facing the space environment, it is likely to be damaged. Meanwhile, the primary mirror is planned to be made of Zerdour, which is a typical brittle and thick material, and its damage is mainly in the form of corrosive pitting. The scattering level of the primary mirror will change significantly after pitting [39], which will cause changes in the PST of the Taiji telescope. Therefore, it is necessary to study the effect of micrometeoroids on the scattering level of the primary mirror of the Taiji telescope.

The NASA SSP30425B model is a commonly used micrometeoroid environment model, which demonstrates the relationships between interstellar micrometeoroid flux and mass [40]. Combining the orbital data of the Taiji Telescope (Lagrange orbit), we can get the predicted value of the number of impacts of micrometeoroids, as shown in Figure 8. It is estimated that the number of micrometeoroid (mass greater than $10 \times 10^{-12}$ g) impacts on the telescope will reach 308 in 4 years, which will increase to 769 in 10 years.

The optical surface is pitted after being impacted by micrometeoroids. Gary L. Peterson et al. [41] proposed a BSDF modeling method for scratches and digs, and this method can also be used for the BSDF modeling of the surface impacted by micrometeoroids. The BSDF of the optical surface is related to the number of impacts $u_D$ and diameter of pits $D$ (as shown in Equation (22)). The diameter $D$ is described by Equation (23), and the values of the parameters in Equation (23) are shown in Table 7 [42]. The BSDF calculated by Equations (22) and (23) is shown in Figure 9. Here, we use the ABg model to describe the BSDF.

$$\text{BSDF}(\theta) = \frac{u_D D^2}{4} \times \left\{ 1 + \frac{\pi^2 D^2}{4\lambda^2} \left[ 1 + \frac{\sin^2(\theta)}{\left(\frac{4}{\pi^4}\right)^{\frac{2}{3}} \left(\frac{\lambda}{D}\right)^2} \right]^{\frac{-3}{2}} \right\} \qquad (22)$$

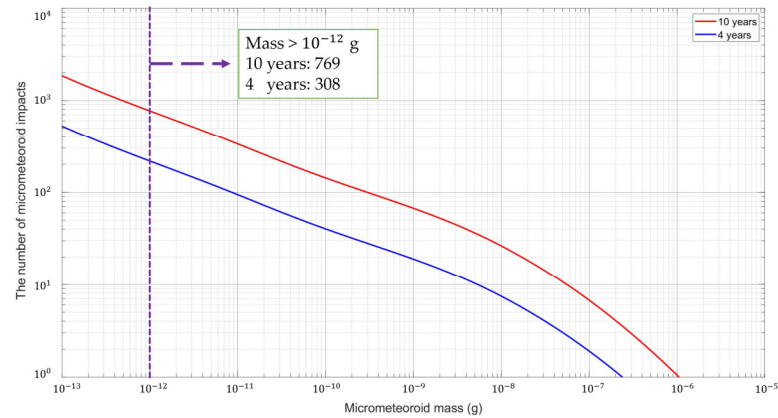$$D_{max} = K_1 K_c d_\mu^\xi \rho_\mu^\beta v^\gamma \rho_t^\kappa \qquad (23)$$



**Figure 8.** Prediction of the number of micrometeoroid impacts. The number of impacts is 308 for 4 years and 769 for 7 years.

**Table 7.** Values of parameters in Equation (23).

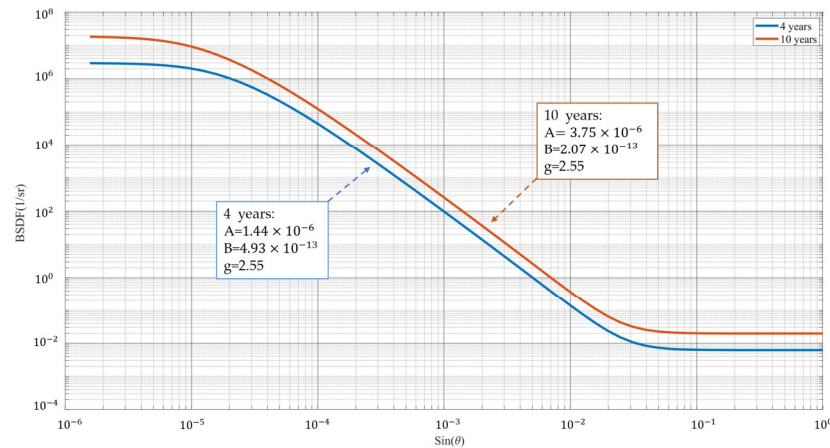| Model Characteristic Factor $K_1$ | Mean Density of Micrometeoroids æ- | fi |
|---|---|---|
| 6.0 | 2.5 g/cm$^2$ | 0.71 |
| Pit factor $K_c$ | Reflector density $\rho_t$ | $\gamma$ |
| 10 | 2.53 g/cm$^2$ | 0.755 |
| Impact velocity $v$ | $\xi$ | $\kappa$ |
| 20 km/s | 1.13 | $-0.5$ |



**Figure 9.** BSDF of the primary mirror after 4 and 10 years of telescope service.

The PST results obtained by assigning the above calculation results to the M1 and maintaining the other mirrors in the ideal optical surface state are shown in Table 8. According to the analysis results, the PST of the optical system is two orders of magnitude lower than the required value, regardless of whether the service life is 4 or 10 years. Therefore, it can be considered that the variation of the scattering level caused by the damage of micrometeoroids can be ignored.

**Table 8.** The changes of PST after the orbiting of the Taiji telescope.

| Years of Service | PST | Years of Service | PST |
|---|---|---|---|
| 1 | $4.45 \times 10^{-13}$ | 6 | $2.82 \times 10^{-12}$ |
| 2 | $1.02 \times 10^{-12}$ | 8 | $4.45 \times 10^{-12}$ |
| 4 | $2.06 \times 10^{-12}$ | 10 | $4.91 \times 10^{-12}$ |

## 5. Conclusions

In this paper, the influence of backscattered light on the phase noise has been firstly analyzed through theoretical derivation. The analysis results have shown that when the point source transmittance (PST) of the optical system is less than $4 \times 10^{-10}$, the phase noise generated by the backscattered light is less than 1 pm, which has met the requirements of the Taiji telescope. Subsequently, we have carried out a detailed stray light analysis of the Taiji Telescope, and have come to the following conclusions:

(1) In the optical system of the Taiji telescope, the third and fourth mirrors were the main scattering sources, accounting for 31.02% and 67.22% of the total scattering energy, respectively. The primary mirror contributed the least to the backscattering energy, accounting for only 0.03%.

(2) The optimal combination of the surface roughness was obtained by analyzing the backscattering caused by the surface roughness. The PST was $3.89 \times 10^{-10}$ when the surface roughness of M1, M2, M3, and M4 were 20 Å, 4 Å, 1 Å, and 1 Å, respectively.

(3) Through the analysis of the backscattering caused by particle contamination, it was obtained that the cleanliness control level of the telescope was required to be better than 300, and the PST of the optical system was $3.55 \times 10^{-12}$ at this condition.

(4) Although the primary mirror of the Taiji telescope should be damaged by the impact of micrometeoroids after entering orbit, the variation of the PST of the Taiji telescope can be neglected because the contribution of the primary mirror to the scattered energy was very small.

In general, the backscattering of the Taiji telescope has a significant impact on the phase noise. The Taiji telescope is required to ensure good environmental cleanliness during installation and storage. For the surface roughness, the M3 and M4 need to be strictly limited. In the future study, we will ultra-smooth the optical surface and measure its BSDF, and finally complete the analysis of scattered light of the Taiji telescope based on the actual measurement data.

**Author Contributions:** Conceptualization, B.S.; methodology, B.S.; software, X.D.; validation, W.S. and W.T.; formal analysis, Y.D.; investigation, B.S.; resources, B.S.; data curation, X.D.; writing—original draft preparation, B.S.; writing—review and editing, W.S.; visualization, W.S.; supervision, W.S.; project administration, W.T.; funding acquisition, Y.D. All authors have read and agreed to the published version of the manuscript.

**Data Availability Statement:** The data presented in this study are available on request from the corresponding author. The data are not publicly available due to privacy.

**Conflicts of Interest:** The authors declare no conflict of interest.

## References

1. Abbott, B.P.; Abbott, R.; Abbott, T.; Abernathy, M.; Acernese, F.; Ackley, K.; Adams, C.; Adams, T.; Addesso, P.; Adhikari, R. Observation of gravitational waves from a binary black hole merger. *Phys. Rev. Lett.* **2016**, *116*, 061102. [CrossRef]
2. Jani, K.; Shoemaker, D.; Cutler, C. Detectability of intermediate-mass black holes in multiband gravitational wave astronomy. *Nat. Astron.* **2020**, *4*, 260–265. [CrossRef]
3. Amaro-Seoane, P.; Audley, H.; Babak, S.; Baker, J.; Barausse, E.; Bender, P.; Berti, E.; Binetruy, P.; Born, M.; Bortoluzzi, D. Laser interferometer space antenna. *arXiv* **2017**, arXiv:1702.00786.

4. Gong, X.; Lau, Y.-K.; Xu, S.; Amaro-Seoane, P.; Bai, S.; Bian, X.; Cao, Z.; Chen, G.; Chen, X.; Ding, Y. Descope of the ALIA mission. In *Journal of Physics: Conference Series*; IOP Publishing: Bristol, UK, 2015; p. 012011.

5. Xue-Fei, G.; Sheng-Nian, X.; Ye-Fei, Y.; Shan, B.; Xing, B.; Zhou-Jian, C.; Ge-Rui, C.; Peng, D.; Tian-Shu, G.; Wei, G. Laser interferometric gravitational wave detection in space and structure formation in the early universe. *Chin. Astron. Astrophys.* **2015**, *39*, 411–446. [CrossRef]

6. Luo, Z.; Guo, Z.; Jin, G.; Wu, Y.; Hu, W. A brief analysis to Taiji: Science and technology. *Results Phys.* **2020**, *16*, 102918. [CrossRef]

7. Ruan, W.-H.; Guo, Z.-K.; Cai, R.-G.; Zhang, Y.-Z. Taiji program: Gravitational-wave sources. *Int. J. Mod. Phys. A* **2020**, *35*, 2050075. [CrossRef]

8. Ziren, L.; Min, Z.; Gang, J.; Yueliang, W.; Wenrui, H. Introduction of Chinese space-borne gravitational wave detection program "Taiji" and "Taiji-1" satellite mission. *J. Deep Space Explor.* **2020**, *7*, 3–10.

9. Luo, Z.; Wang, Y.; Wu, Y.; Hu, W.; Jin, G. The Taiji program: A concise overview. *Prog. Theor. Exp. Phys.* **2021**, *2021*, 05A108. [CrossRef]

10. Wu, B.; Huang, C.-G.; Qiao, C.-F. Analytical analysis on the orbits of Taiji spacecrafts to infinite order of the orbital eccentricity. *Phys. Rev. D* **2020**, *101*, 064049. [CrossRef]

11. Chen, S.; Jiang, H.; Wang, C.; Chen, Z. Optical System Design of Inter-Spacecraft Laser Interferometry Telescope. *Opt. Photonics J.* **2019**, *9*, 26–37. [CrossRef]

12. Livas, J.; Sankar, S.; West, G.; Seals, L.; Howard, J.; Fitzsimons, E. eLISA Telescope In-field Pointing and Scattered Light Study. In *Journal of Physics: Conference Series*; IOP Publishing: Bristol, UK, 2017; p. 012015.

13. Sankar, S.R.; Livas, J.C. Initial progress with numerical modelling of scattered light in a candidate eLISA telescope. In *Journal of Physics: Conference Series*; IOP Publishing: Bristol, UK, 2015; p. 012031.

14. Livas, J.C.; Arsenovic, P.; Crow, J.A.; Hill, P.C.; Howard, J.M.; Seals, L.T., III; Shiri, S. Telescopes for space-based gravitational wave missions. *Opt. Eng.* **2013**, *52*, 091811. [CrossRef]

15. Sankar, S.R.; Livas, J.C. Optical telescope design for a space-based gravitational-wave mission. In Proceedings of the Space Telescopes and Instrumentation 2014: Optical, Infrared, and Millimeter Wave, Montreal, QC, Canada, 22–27 June 2014; pp. 283–289.

16. Landini, F.; Riva, A.; Gai, M.; Baccani, C.; Focardi, M.; Pancrazzi, M. Stray light evaluation for the astrometric gravitation probe mission. In Proceedings of the Optical and Infrared Interferometry and Imaging V, Edinburgh, UK, 27 June–1 July 2016; pp. 943–953.

17. Schröder, S.; Duparré, A.; Coriand, L.; Tünnermann, A.; Penalver, D.H.; Harvey, J.E. Modeling of light scattering in different regimes of surface roughness. *Opt. Express* **2011**, *19*, 9820–9835. [CrossRef] [PubMed]

18. Lightsey, P.A.; Atkinson, C.B.; Clampin, M.C.; Feinberg, L.D. James Webb Space Telescope: Large deployable cryogenic telescope in space. *Opt. Eng.* **2012**, *51*, 011003. [CrossRef]

19. Abbey, A.; Ambrosi, R.; Wells, A. Effects of micrometeoroid and space debris impacts in grazing incidence telescopes. In Proceedings of the Space Telescopes and Instrumentation II: Ultraviolet to Gamma Ray, Orlando, FL, USA, 24–31 May 2006; pp. 1054–1063.

20. Strüder, L.; Aschenbach, B.; Bräuninger, H.; Drolshagen, G.; Englhauser, J.; Hartmann, R.; Hartner, G.; Holl, P.; Kemmer, J.; Meidinger, N. Evidence for micrometeoroid damage in the pn-CCD camera system aboard XMM-Newton. *Astron. Astrophys.* **2001**, *375*, L5–L8. [CrossRef]

21. Sang, B.; Deng, X.; Peng, B.; Tao, W.; Sha, W. Dimensional Stability Ground Test and in-Orbit Prediction of SiC Telescope Frame for Space Gravitational Wave Detection. *IEEE Access* **2022**, *10*, 21041–21047. [CrossRef]

22. Sasso, C.; Mana, G.; Mottini, S. The LISA interferometer: Impact of stray light on the phase of the heterodyne signal. *Class. Quantum Gravity* **2019**, *36*, 075015. [CrossRef]

23. Liang, X.; Jianke, Z.; Xun, X.; Yan, Z.; Feng, L. PST research and measurement of lunar-based optical telescope stray light. *Infrared Laser Eng.* **2014**, *43*, 1289–1295.

24. Wuehrer, C.; Birkl, R.A.; de Zoeten, P.; Frey, A.; Hoelzle, E.; Ruehe, W.; de Chambure, D.; van Katwijk, K. PST measurements and wide-angle straylight analyses of the XMM (X-Ray Multi Mirror) telescopes. In Proceedings of the X-Ray Optics, Instruments, and Missions III, Munich, Germany, 27–29 March 2000; pp. 113–122.

25. Wang, G.; Xing, F.; Wei, M.; You, Z. Rapid optimization method of the strong stray light elimination for extremely weak light signal detection. *Opt. Express* **2017**, *25*, 26175–26185. [CrossRef]

26. Clermont, L.; Aballea, L. Stray light control and analysis for an off-axis three-mirror anastigmat telescope. *Opt. Eng.* **2021**, *60*, 055106. [CrossRef]

27. Sholl, M.; Grochocki, F.; Fleming, J.; Besuner, R.; Jelinsky, P.; Lampton, M. Stray light design and analysis of the SNAP telescope. In Proceedings of the Optical Modeling and Performance Predictions III, San Diego, CA, USA, 29–30 August 2007; pp. 128–139.

28. Asadnezhad, M.; Eslamimajd, A.; Hajghassem, H. Stray light analysis, baffle, and optical design of a high-resolution satellite camera. *J. Appl. Remote Sens.* **2018**, *12*, 026009. [CrossRef]

29. Zeng, J.; Butler, J.J.; Xiong, X.; Thompson, A.K.; Bousquet, R. BSDF measurements and analyses of specular samples using a table-top goniometer in support of remote sensing instruments. In Proceedings of the Reflection, Scattering, and Diffraction from Surfaces VII, San Diego, CA, USA, 23–27 August 2020; pp. 13–23.

30. Hale, R.R. Optical stability of diffuse reflectance materials in space. In Proceedings of the Reflective and Refractive Optical Materials for Earth and Space Applications, Orlando, FL, USA, 4–5 April 1991; pp. 173–182.

31. Peterson, G.L. Analytic expressions for in-field scattered light distributions. In Proceedings of the Optical Modeling and Performance Predictions, San Diego, CA, USA, 6–7 August 2004; pp. 184–193.

32. Greynolds, A.W. Relative micro-roughness scattering from the surfaces of a transmitting optical element. In Proceedings of the Stray Radiation IV, San Diego, CA, USA, 20 August 1985; pp. 35–37.

33. Hubbard, R. M1 Microroughness and Dust Contamination. Available online: https://dkist.nso.edu/sites/atst.nso.edu/files/docs/TN-0013-D.pdf (accessed on 10 November 2022).

34. Spyak, P.R.; Wolfe, W.L. Scatter from particulate-contaminated mirrors. part 3: Theory and experiment for dust and lambda = 10.6 um. *Opt. Eng.* **1992**, *31*, 1764–1774. [CrossRef]

35. Dittman, M.G. Contamination scatter functions for stray-light analysis. In Proceedings of the Optical System Contamination: Effects, Measurements, and Control VII, Seattle, WA, USA, 9–11 July 2002; pp. 99–110.

36. IEST-STD-CCD IS. *Product Cleanliness Levels and Contamination Control Program*; Institute for Environmental Science and Technology (IEST): Rolling Meadows, IL, USA, 2002.

37. Chylek, T.; Hansen, E.R.; Sherman, R.; Matthews, P.; Hyde, T. Design of the automated $CO_2$ optics cleaning system for the Thirty Meter Telescope. In Proceedings of the Advances in Optical and Mechanical Technologies for Telescopes and Instrumentation IV, Online, 14–18 December 2020; pp. 920–931.

38. Ma, P.T.; Fong, M.C.; Lee, A.L. Surface particle obscuration and BRDF predictions. In *Scatter from Optical Components*; SPIE: Bellingham, WA, USA, 1990; pp. 381–391.

39. Khodnevych, V.; Lintz, M.; Dinu-Jaeger, N.; Christensen, N. Stray light estimates due to micrometeoroid damage in space optics, application to the LISA telescope. *J. Astron. Telesc. Instrum. Syst.* **2020**, *6*, 048005. [CrossRef]

40. Torky, M.; Hassanein, A.E.; El Fiky, A.H.; Alsbou, Y. Analyzing space debris flux and predicting satellites collision probability in LEO orbits based on Petri nets. *IEEE Access* **2019**, *7*, 83461–83473. [CrossRef]

41. Peterson, G.L. A BRDF model for scratches and digs. In Proceedings of the Reflection, Scattering, and Diffraction from Surfaces III, San Diego, CA, USA, 13–16 August 2012; pp. 107–116.

42. Li, Y. Damage Behavior of Dust Particles Impinging on Optical Glass at High Speed. Master's Thesis, HIT, Harbin, China, 2009.